Military Technical College
Kobry El-Kobbah,
Cairo, Egypt

6th International Conference
on
Chemical & Environmental
Engineering
29 -31 May, 2012.

ENMA-1

BALLISTIC PROPERTIES PREDICTION FOR VARIANT BUTALITES COMPOSITIONS, AN EASY ABSTENTION TECHNIQUE

W. Abdel-Wareth[1], X. Xu[2]

Abstract

Ballistic properties for variant Butalites formulations based on Ammonium perchlorate (AP) and hydroxy terminated polybutadiene with some other additives were practically investigated then theoretically predicted. The predictions were investigated for formulations with burning rates ranging from 0.26 to 17.94 mm/sec at 70 bar. The predictions were performed using the developments applied to the basic model of multiple flames, the BDP model. The developments were established over the model equations using an easy abstention technique, without multiple flame standoff distances. The results were verified by considering AP regression as the rate-controlling step in combustion, by introducing the additives to the model equations in a passive technique, by the use of a one-dimensionally limited temperature profile to estimate the propellant surface temperature, and by solving the combustion equations iteratively for the mass flux and surface temperature until they reached the required convergence. A computer program was established for obtaining the linear burning rate, surface temperature and other ballistic properties of the previous formulations. The results showed that the predicted linear burning rates were acceptable and verified the international acceptance margins in this field.

Key Words: Composite propellants; Combustion; Ballistic properties; Linear Burning rate

[1] Egyptian Armed Forces (awael972000@yahoo.com)
[2] Professor (xuxu@buaa.edu.cn)
School of Astronautics, BUAA, Beijing 100191, China

1 Introduction

Investigation of composite propellant burning operations involves complex phenomena occurring in solid, liquid and gas phases where physical and chemical processes that occur during their combustion are not fully understood [1]. All ballistic properties predictions (Linear burning rate, pressure exponent and temperature sensitivities) for a composite propellant using one combustion mechanism encounter complicated operations. The linear burning rate represents the base foundation to start any modifications (augmentations) to the solid motor ideal performance due to its design constraints [2]. In this paper, linear burning rate prediction means modeling of the combustion phenomenon with steady state burning under zero cross-flow situations over the solid phase, combustion zone and gas phase [3].

The international goal is the development of a universal model, which can predict propellant grain composition from burning rate requirements. This is a tall order in view of the complex competing reactions taking place simultaneously and the problems associated with probing thin reaction zones precisely. Therefore, the problems division into small parts for clearer investigations seems to be an appropriate way to achieve progress in the field. Understanding the combustion of a composite propellant is a serious challenge even without the addition of burning rate modifiers or metallic fuels, and yet it is crucial to understand the former in order to understand the latter. Adding to the complexity of composite propellant combustion is the fact that it is an inherently three-dimensional and intrinsically unsteady system, even when the macroscopic environment is steady. Yet, without complete understanding of all the areas affecting combustion on a microscopic level, no computer code would be able to validate propellant combustion [4-7]. Therefore, a return to the fundamentals is necessary and the modifications of a trusty combustion model to verify the international acceptance margins between the theoretical and practical results will be an applicable way.

Performance prediction for composite propellants is very important, as it is the principal method by which the difference between the theoretically predicted and practically evaluated parameters is minimized. The international acceptance margins between the theoretical predictions and practical evaluations must be applied. In this paper, the international acceptance margins are verified if minimum of 90% of the predicted linear burning rates at 70 bar are within ± 10% error range when compared to the experimental results [8].

The objective of this study was to investigate a technique for the ballistic properties prediction of a specific composite propellant family (specific ingredients with pre-defined specifications) under specific pressure interval. The propellant family (Butalites [9]) was based on ammonium perchlorate (AP), polyurethane binder (PU), aluminum powder (Al), carbon black (CB), calcium carbonate ($CaCO_3$) and copper chromite (CC). The polyurethane binder matrix was composed of hydroxy terminated polybutadiene (HTPB) pre-polymer with anti-oxidant (cyanox), hexamethylene diisocyanate (HMDI) as a curing agent, methyl aziridinyl Phosphine oxide (MAPO) as a bonding agent and diisooctyl azelate (DOZ) as a plasticizer. Herein, our prime importance was to predict the linear burning rates of variant Butalites formulations, without solid motor complexities. The combustion pressure under investigation was defined as 20-120 bar. Our effort involved the use of FORTRAN programs concerning analysis of the propellant solid and gas phases, which was then followed by inspection over the combustion zone modeling modifications with the aid of thermal analytical measurements (TAM), specific surface area measurements and ignition temperature (T_{ig}) measurements. These measurements were applied for the used ingredients and some mixtures.

2 Practical data survey

At this stage, the practical data was divided into two main categories. The first (Table 1) included the practical measurements applied for 20 Butalites formulations. The formulations were prepared (using 1-gallon capacity mixer) according to factors affecting combustion using the previous ingredients. Their burning rates were measured by using the Crawford bomb (Group-A) and 2×4 ballistic evaluation motor (Group-B) techniques. The second data category (Tables 2 and 3) included the practical measurements applied for the used ingredients. The ingredients were subjected to TAM, differential scanning calorimetry (DSC)/thermal gravimetric analysis (TGA), using the simultaneous analyzer SDT-Q600 V20.5 under dynamic nitrogen atmosphere and heating rate of 40 ºC/min. In addition, the solid ingredients were subjected to specific surface area measurements using the NOVA 2200e-WIN2 V2.1 apparatus where the Brunauer-Emmett-Teller (BET) method was applied. Moreover, special mixtures were subjected to T_{ig} measurements under heating rate of 40 ºC/min. The DSC/TGA digital data were used to determine the decomposition characteristic parameters of the ingredients (heats associated with any process of change, AP kinetic parameters, binder kinetic parameters, AP heat of gasification and binder heat of pyrolysis). The kinetic parameters were calculated by using a simple FORTRAN computer program based on the modified isoconversional method. The calculations were inspected at two intervals. The first was the low conversion interval at 5 to 30% for both AP and binder. The second was the high conversion interval at 30 to ~70% for AP and 30 to ~95% for binder [10, 11]. AP heat of gasification and binder heat of pyrolysis were determined automatically, using the Universal Analysis 2000 data acquisition system linked to the SDT-Q600, on the basis of a hypothetical approach [12]. The parameters of AP were investigated as a function of its particle size and for the binder as a function of its formulation curative ratios [NCO/OH (R1), IMINE/OH (R2) and DOZ/HTPB (R3)].

Table 1 Prepared formulations and their measured results

No.	Binder %	AP 419.5 µm %	AP 175 µm %	AP 54.2 µm %	AP 9 µm %	Al 11.5 µm %	CC 0.75 µm %	$CaCO_3$ 14 µm %	CB 10 µm %	ρ_P (g/cm^3)	r at 70 bar (mm/s) -30 °C	25 °C	50 °C	n
AI-	74.5				25				0.	1.085		0.26	0.36	0.1
AI-	64.5				35				0.	1.174		0.53	0.58	0.2
AI-	54.5				45				0.	1.245	0.79	1.11	1.26	0.3
AII-	54.5			15	30				0.	1.246		1.01	1.19	0.2
AII-	54.5			30	15				0.	1.248		0.89	1.02	0.3
AIII	44.5				45	10			0.	1.351	2.17	2.56	2.82	0.2
AIII	34.5				45	20			0.	1.492	3.82	4.15	4.37	0.2
AIV	51.5				45		3		0.	1.280	1.42	1.71	2.08	0.2
AIV	48.5				45		6		0.	1.339	1.85	2.36	2.81	0.2
AV-	41.5				45	10	3		0.	1.392	2.67	3.15	3.37	0.1
AV-	38.5				45	10	6		0.	1.456	3.29	3.75	4.06	0.2
BI-1	20		31.		31.	17						6.81		0.3
BI-2	16		33.		33.	17						7.40		0.3
BI-3	12		35.		35.	17						10.0		0.4
BII-	14	40	18		10	18				1.762	6.27	6.75	6.98	0.3
BII-	14	18	40		10	18				1.762	6.89	7.38	7.62	0.2
BIII	19		40	20	20				1	1.635	6.92	7.75	8.16	0.4
BIII	18		40	20	20		1		1	1.652	10.9	11.9	12.4	0.3
BIII	18		40	20	20			1	1	1.645	6.86	7.18	7.33	0.3

BIV	16	22	12	34	14	2	1.714	17.9	0.2

Table 2 Ingredients description, specific surface areas and TAM results

No.	Sample description	Practical specific surface (m^2/g)	Theoretical specific surface (m^2/g)	Property / Value (cal/g)	(Low) A (/s)	(Low) E (kcal/mole)	(High) A (/s)	(High) E (kcal/mole)
1	AP (10	0.56	0.31	Q_r /101.9	5.16×1	24.26	5.14×10	27.11
2	AP (22.5	0.37	0.14	Q_L /111.0	2.52×1	22.98	4.66×10	26.99
3	AP (82.5	0.19	0.04	Q_L /112.7	1.21×1	21.67	3.86×10	26.73
4	AP (196	0.13	0.02	Q_L /117.1	2.86×1	19.24	3.25×10	26.51
5	AP (390	0.09	0.01	Q_L /118.3	2.07×1	18.50	3.14×10	26.48
6	CB (10	7.66	0.32					
7	Al (11.5	0.78	0.19	h_f /92.3				
8	CC (0.75	14.94	1.29					
9	$CaCO_3$	1.65	0.16	Q_{caco3}/263				
10	PU			Q_{fuel}	7.45×1	31.96	3.70×10	45.26
11	PU			Q_{fuel}	1.75×1	29.83	3.09×10	44.93
12	PU			Q_{fuel}	2.20×1	30.21	3.24×10	45.02
13	PU			Q_{fuel}	1.19×1	25.45	2.42×10	44.52

Table 3 Special mixtures prepared for T_{ig} measurements and their results

No.	PU-binder Sample No. 10	AP 22.5 µm	AP 82.5 µm	AP 390 µm	CB 10 µm	Al 11.5 µm	CC 0.75 µm	$CaCO_3$ 14 µm	T_{ig} (ºC)
1	30	70							355
2	50		50						356
3	37.5		62.5						355
4	30		70						354
5	30			70					353
6	30		62.5		7.5				352
7	30		50			20			349
8	30		62.5				7.5		317
9	30	62.5					7.5		304
10	30		62.5					7.5	358
11	30	62.5						7.5	362

3 Solid phase data survey

At this stage, the propellant solid phase specifications were inspected by creating two FORTRAN computer programs based on the basic international concepts in this field beside basic mathematics and dependent on the raw materials specifications. The first one (Table 4) was concerned with binder composition analysis. It was investigated the binder composition, summary formula, enthalpy of formation and density. The second one (Table 5) was concerned with propellant composition analysis. It was investigated the propellant density, thermal properties [13, 14], cast-ability margins [15], fillers volumetric loading factors and surface areas.

Table 4 Data for 100% binder compositions

Binder formulations	Binder (%)	ΔH_{fuel} (cal/g)	Main data estimated			HTPB%	HMDI%	DOZ%	MAPO%	ρ_f (g/cm^3)
			R_1	R_2	R_3					
Group (A)	34.5/74.5	-71.2737	2	0.817	0	83.6913	11.9725	0.0	4.3362	0.9288
Sub-group (BI)	12-20	-194.746	0.7	0.5	0.25	75.0876	3.7596	18.7719	2.3809	0.9166
Sub-group (BII)	14	-193.816	0.72	0.45	0.25	75.1858	3.8721	18.7965	2.1456	0.9164
Sub-group (BIII)	18-19	-197.958	0.825	0.6	0.25	74.2357	4.3807	18.5589	2.8247	0.9159
Sub-group (BIV)	16	-216.557	0.75	0.334	0.3	72.7364	3.9020	21.8209	1.5407	0.9157

Table 5 Solid phase analysis results

No.	Modified idealized surface		Solid density (g/cm^3)	Thermal conductivity (cal/cm.s.K)	Specific heat (cal/g.K)	Initial non-idealized			Cast-ability margins
	$\frac{\overline{S_{ox}}}{S_\circ}$	$\frac{\overline{S_{ox}}}{\overline{S_{ox}}+S_f}$				Binder (cm^2)	AP (cm^2)	Propellant (cm^2)	
AI-1	2.068628E-	2.187174E-01	1.0747	0.00061	0.4696	0.842	0.353	1.288	within
AI-2	2.968999E-	3.143678E-01	1.1436	0.00065	0.4414	0.766	0.527	1.391	within
AI-3	3.915885E-	4.152584E-01	1.2219	0.00070	0.4133	0.679	0.723	1.508	within
AII-	3.405868E-	3.630130E-01	1.2219	0.00070	0.4133	0.679	0.581	1.365	within
AII-	2.802587E-	3.005231E-01	1.2219	0.00070	0.4133	0.679	0.438	1.222	within
AIII-	3.896379E-	4.707039E-01	1.3367	0.00081	0.3807	0.593	0.791	1.734	within
AIII-	3.877070E-	5.432380E-01	1.4754	0.00097	0.3481	0.490	0.873	2.008	within
AIV-	2.395778E-	4.301028E-01	1.2641	0.00073	0.4011	0.661	0.748	2.793	within
AIV-	1.725828E-	4.460478E-01	1.3094	0.00077	0.3889	0.642	0.775	4.171	within
AV-	2.388463E-	4.898687E-01	1.3875	0.00085	0.3685	0.570	0.821	3.154	within
AV-	1.722029E-	5.106602E-01	1.4422	0.00090	0.3563	0.545	0.854	4.686	within
BI-1	4.790463E-	6.663880E-01	1.6559	0.00095	0.2789	0.281	0.842	1.617	within
BI-2	5.278049E-	7.447003E-01	1.7217	0.00103	0.2737	0.213	0.931	1.657	within
BI-3	5.802450E-	8.314757E-01	1.7929	0.00111	0.2685	0.139	1.027	1.701	boundary
BII-	3.592687E-	6.332042E-01	1.7608	0.00108	0.2708	0.178	0.462	1.197	within
BII-	3.793089E-	6.535029E-01	1.7608	0.00108	0.2708	0.178	0.503	1.237	within
BIII-	5.355779E-	6.947540E-01	1.6257	0.00088	0.2825	0.233	0.796	1.370	within
BIII-	3.968822E-	7.115514E-01	1.6505	0.00090	0.2799	0.218	0.808	1.927	within
BIII-	5.240839E-	7.120010E-01	1.6449	0.00090	0.2805	0.217	0.805	1.428	within
BIV	3.433132E-	7.561200E-01	1.7293	0.00101	0.2709	0.215	0.998	2.800	within

4 Gas phase data survey

At this stage, the propellant gas phase specifications were inspected using the thermo-chemical calculations methodology at 70 bar. This stage was very important for the main purpose of this study where, specifications, calculations deviations were not allowed and cannot be practically compared. Therefore, the use of a trusty code, to verify that objective, was more suitable and recommended. The international FORTRAN Code of Gordon and Mc Bride developed by NASA Research Center (CEA-2 Code, 2004) [16] was used to calculate the formulations gas phase characteristic specifications under assigned enthalpy and pressure conditions (Table 6).

Table 6 Analysis results by the CEA-2 Code at 70 bar

No.	Thermal properties assuming frozen reactions		Combustion temperature (K)
	Conductivity × 10^{-3} (cal/cm.s.K)	Specific heat (cal/g.K)	
AI-1	0.5290	0.7926	1173.65
AI-2	0.5197	0.6848	1224.20
AI-3.	0.5017	0.5972	1273.29
AIII-1	0.8862	0.6230	1918.35
AIII-2	1.0759	0.6659	2368.64
AIV-1	0.5000	0.5901	1279.64
AIV-2	0.4980	0.5829	1286.30
AV-1	0.8712	0.6405	1944.07
AV-2	0.8546	0.6175	1970.64
BI-1	0.9448	0.5016	2813.11
BI-2	0.9491	0.4997	3241.24
BI-3	0.9859	0.4823	3527.42
BII	0.9965	0.4933	3409.35
BIII-1	0.5970	0.4480	2425.12
BIII-2	0.6006	0.4441	2497.06
BIII-3	0.5983	0.4445	2483.94
BIV	0.9105	0.4853	3169.77

5 Used technique and BDP model modifications

5.1 Principal view

The burning rate of a solid propellant is primarily influenced by its formulation with the characteristics of each forming component. From the combustion models, the basic Beckstead, Derr and Price (BDP) model using multiple flames [17] appears to be rather satisfying from many points of view. It has been used in many research programs since 1970 [18-22]. There appear, however, certain complexities in the BDP model such as the determination of the standoff distances of the multiple flames that sometimes limit somewhat its day-to-day utility [20]. The difficulty here arises as much from the nature of the relevant mathematical expressions as from a lack of precise information regarding the values of the parameters involved. Under such circumstances, it seems worthwhile to make the approach a little more simplified. This will perhaps enable the model liberate itself from its emphasis on the flame standoff distances. No doubt in this process, the technique is liable to become less sophisticated, but it will be easier to operate and this is precisely what may be warranted when new propellants will be developed by their pre-inspected constituents.

The aim of the this stage was to describe modifications of the basic BDP model suitable for such a simplified theory by the use of an easy abstention technique for a known composite propellant family with pre-defined ingredients on the basis of a specific combustion pressure value of 70 bar, covered the interval from 20 to 120 bar.

It was very important to clarify the following points:

1) The problem was handled separately for each formulation over its solid phase (zone-1), combustion zone [zone-2, decomposition phase (at the combustion sub-surface) and condensed phase (solid gas interface, at or just above the combustion surface)] and gas phase (zone-3).
2) The BDP model simplified theory was concerned with the carelessness of both flame standoff distances and dependence of the flame structure on AP particle size.

3) The physical meaning of the applied modifications was the treatment methodology of the multi-modal AP systems, CB, Al and burning rate modifiers incorporation into the model equations.

4) This problem was treated by the use of a one-dimensional limited temperature profile, (the limitation here means that it was not dependent on the reaction zones thicknesses), Figure 1 [4, 23].

5) The multi-modal oxidizer surface areas were mainly based on the practical data applied by the BET-method using the Sauter mean diameter for each AP grade involved in each formulation.

5.2 Combustion zone treatments

It was very important to apply a clear treatment technique for the measured parameters and calculated specifications to be ready for the required applications using the basic BDP model modifications at the combustion zone. This objective was achieved by the collection of each set of data to form the best-fit equation describing it. The treatment technique for the 20 Butalites formulations was achieved by the following steps (Figure 1):

1) For the solid phase, far inside the propellant ($T \approx T_o$, initial temperature), the specifications introduced as they were calculated (from the solid phase data survey). At the solid-phase/decomposition-phase imaginary boundary interface, the thermal properties were corrected under the assumption of a constant propellant solid density. This principle formed an approach to the propellant combustion surface. The boundary interface temperature was suggested to, approximately, equal the average value between T_o and T_s (surface temperature) and named the decomposition temperature T_d.

2) To reach the solid phase thermal properties at $T \approx T_d$ and to keep away from the complicated heat transfer mechanisms, an abridged method was used. It was based on the trusty definition of each thermal property versus temperature for each material involved in the propellant matrix [14]. Thus, we recalculated the propellant thermal properties at $T \approx T_d$ using the solid phase programs. For the interval $T \approx T_d \sim T_s$, the decomposition characteristic parameters were treated and evidently presented at Appendix 1.

3) For the gas phase, far outside the propellant combustion surface ($T \approx T_f$, flame temperature), the specifications introduced as they were calculated (from the gas phase data survey).

4) To reach the gas phase thermal properties at $T \approx T_{fs}$ (as an approach to the combustion surface) and to keep away from the complicated heat transfer mechanisms, also an abridged method was used. For each formulation, interpolations were used to describe each property variation (from T_f to T_s) for an imaginary temperature value near the combustion surface. Thus, it was easily applied to define the property variation at any temperature within the predefined interval. The imaginary temperature approach (T_{fs}) was assumed to have an incremental value, approximately, equal to the same difference between T_s and T_d:

$$T_{fs} \approx 2T_s - T_d \qquad (1)$$

5.3 Ingredients incorporation

We applied systematic modifications to the basic BDP model combustion equations [17]. Following the BDP model:

5.3.1 AP/PU-binder based propellant

Mass burning rate was re-expressed as an averaged one-step Arrhenius function for different AP grades ($\overline{m_{ox}}$):

$$\overline{m_{ox}} = \sum_{i=1}^{n} \alpha_{ox_i} m_{ox_i} = \sum_{i=1}^{n} \alpha_{ox_i} \rho_{ox} r_{ox_i} = \sum_{i=1}^{n} \alpha_{ox_i} A_{ox_i} \exp\left(-E_{ox_i} / RT_s\right) \quad (2)$$

The surface temperature T_s was assumed uniform and obtained from an energy balance at the propellant combustion surface. Thus,

$$m_T C_p (T_s - T_\circ) = -\overline{m_{ox}} \frac{\overline{S_{ox}}}{S_\circ} \overline{Q_L} - m_f \frac{S_f}{S_\circ} Q_{fuel} + \beta_F Q_{PF} m_T \exp\left(-\xi^*_{PF}\right) + (1-\beta_F)\overline{m_{ox}} \times \frac{\overline{S_{ox}}}{S_\circ}\left[\overline{Q_{AP}} \exp\left(-\overline{\xi^*_{AP}}\right) + Q_{FF} \exp\left(-\xi^*_{FF}\right)\right] \quad (3)$$

Where:

$$\frac{\overline{S_{ox}}}{S_\circ} = \sum_{i=1}^{n} \frac{\alpha_{ox_i} S_{ox_i}}{S_\circ} \quad (4)$$

$$\overline{Q_L} = \sum_{i=1}^{n} \alpha_{ox_i} Q_{L_i} \quad (5)$$

$$\overline{Q_{AP}} = C_{AP}(T_{AP} - T_\circ) + \overline{Q_L} \quad (6)$$

Equation (3) described the heat transferred from the various flame fronts (the pre-mixed AP monopropellant flame, the primary flame between the decomposition products of the oxidizer and the binder, and the final diffusion flame between the products of the monopropellant flame and the binder decomposition products) to the solid surface as presented at Figure 2. The multiplying factor represented the heat flux generated by the flame front, while the exponential function represented the generated heat conducted fraction back to the combustion surface. The parameters $\overline{S_{ox}}$, $\overline{Q_L}$, $\overline{Q_{AP}}$ and $\overline{\xi^*_{AP}}$ related to the averaged values of the multi-modal AP systems.

To overcome the uncertainties in the determination of the various parameters occurring in the BDP model flame equations, it was assumed as suggested by Summerfield et al [20, 24] that the overall heat feedback from the flamelets to the surface in the combustion of a non-aluminized propellant is approximately 1.25 times that from the AP monopropellant flame. Under these conditions, Equation (3) was modified to the simpler form:

$$m_T C_p (T_s - T_\circ) = -\overline{m_{ox}} \frac{\overline{S_{ox}}}{S_\circ} \overline{Q_L} - m_f \frac{S_f}{S_\circ} Q_{fuel} + 1.25(1-\beta_F)\overline{m_{ox}} \times \frac{\overline{S_{ox}}}{S_\circ} \times \overline{Q_{AP}} \exp\left(-\overline{\xi^*_{AP}}\right) \quad (7)$$

From the relation:

$$m_T = \left(\overline{m_{ox}} / \alpha\right)\left(\frac{\overline{S_{ox}}}{S_\circ}\right) = \left(\frac{m_f}{(1-\alpha)}\right)\left(\frac{S_f}{S_\circ}\right) \quad (8)$$

Then by substitution into Equation (7) and solution for T_s, the result was:

$$T_s = T_\circ - \alpha \frac{\overline{Q_L}}{C_p} - (1-\alpha)\frac{Q_{fuel}}{C_p} + 1.25(1-\beta_F)\alpha \times \frac{\overline{Q_{AP}}}{C_p} \exp\left(-\overline{\xi^*_{AP}}\right) \quad (9)$$

Where $\overline{\xi^*_{AP}}$ was given by the gas phase kinetic equation:

$$\overline{\xi^*_{AP}} = C_p \overline{m_{ox}}^2 / \lambda k_{AP} P^\delta \quad (10)$$

The reaction rate constant KAP in Equation (10) is an Arrhenius function for the oxidizer dependent on pressure, AP flame temperature and the reaction order (σ). KAP is (calculated from known, well-inhibited samples, AP burning rates at 70 atm [3, 17 and 18]) reported in many references by the value 1.12 g/cm3 s atm(1.8).

To keep away from the standoff distances determinations was a principle in this study. At the same time, the value of β_F was dependent on these flame heights in the BDP model. Therefore, another acceptable solution for this problem was required. β_F values of a typical AP/PS and AP/PU based propellants with 70% AP loadings ($\alpha = 0.7$, for different AP sizes from 5 to 310 μm) and different pressures up to 1000 psi were recorded [25].
To make a connection between these data and our requirements where the structural mode of the HTPB pre-polymer with HMDI in this study represented a PU matrix, the relationship between the pressure [X (psi)] and β_F [Y] ($\alpha = 0.7$) was fitted to the following equation:

$$Y = 307.45\, X^{-1.3113} \rightarrow R^2 = 0.9946 \quad (11)$$

Thus, for any formulation at the interval of 20-120 bar, the new (β_F) value (say β^*_F) corresponded to any new AP (α) value (say α^*) was obtained from the equation:

$$\beta_F^* = \beta_F \left(\frac{1-\alpha^*}{1-\alpha}\right)\frac{\alpha}{\alpha^*} \quad (12)$$

Equations (2, 9, and 10) were solved simultaneously for the AP mass flux, surface temperature, and AP non-dimensional flame stand of distance. The mass flux averaged over the entire propellant surface, where the oxidizer regression was considered as the rate-controlling step in combustion, was represented by:

$$m_T = \left(\overline{m_{ox}} / \alpha\right) \times \left(\frac{\overline{S_{ox}}}{S_\circ}\right) \quad (13)$$

Thus, linear burning rate (r) evaluation for the propellant was given by:

$$r = m_T / \rho_P \quad (14)$$

Treatment of the oxidizer to propellant surface ratio (S_{ox}/S_o) was started from the initial data listed at Table 5. the S_{ox}/S_o was based on the solid ingredients specific surface measurements and the assumption that the homogeneously mixed AP particles for each grade incorporated in the propellant were spheres with initial Sauter mean diameter D_{oi}. This surface was assumed as the non-idealized one before combustion to feel formulation effect on the geometry data.
The previously measured specific surface areas by the BET-method for the solid ingredients cannot be compared to their theoretically determined values (Table 2). Therefore, the start from a criterion based on fixed surface parameters under assumed conditions (specific geometry and pressure) provided us with the required light to handle this situation.
The factor h/D_o in the BDP model represented the fractional distance the oxidizer protruded above or recessed below the surface. It was written by the following equation:

$$\frac{h}{D_\circ} = \frac{1}{2}\left(1 \pm \frac{1}{(3)^{1/2}}\right)\left(1 - \frac{r_{ox}}{r_f}\right) + r_{ox}\frac{t_{ign}}{D_\circ}$$

$$\underline{Where} \quad t_{ign} = C_{ign}\frac{D_\circ^{m^*+1}}{P^{n^*}} \quad \underline{and} \quad r_f = A_f \exp(-E_f / RT_s) \quad (15)$$

Many experimental studies indicated that h/D_o might be positive at low pressures, zero somewhere in the range of 300 to 600 psi and negative at higher pressures [17, 26]. In addition, in the BDP model, variations in the value of oxidizer to propellant surface ratio were determined to have a minor effect on the burning rate curve. Varying t_{ign} in Equation (15) over a very large range of values had a significant effect on the calculated values of h/D_o, a lesser effect on the value of S_{ox}/S_o and virtually no effect on the burning rate. Thus, the parameters involved only in Equation (15), (i.e. A_f, E_f and t_{ign}), had such a small influence on the burning rate that the particular value used for these parameters was not important. These

parameters were adjusted to give consistent values of h/D_o [17]. Therefore, the start from an AP particle domed over or recessed under the binder surface by the value ≈ 0.25 then idealizing it represented our suggested solution for this problem (Figure 3).

The previous suggestion was applied for each AP grade through an imaginary approach based on the conversion of the particle spherical geometry to a cylindrical one with the same diameter D_{oi} and corrected length of $[(2/3)D_{oi}]$. Then, the initial particle volume maintained constant. Under the assumption of unchanged binder volume, the oxidizer volumetric loading fraction was not changed. This operation followed by the definition of a fixed surface unit based on the maximum AP grade diameter $[(2/3)D_{max}]$ in the mixture matrix as the main combustion-controlling factor. This controlling factor was internally controlled by the repeated AP minimum grade diameter $[(2/3)D_{min}]$. Thus, the mixture surface was not represented by the initial area only but by the accumulated surfaces inside its fixed unit. In addition, the accumulated binder surface was a function of its initial value multiplied by the number of its layers inside the fixed unit (D_{max}/D_{min}). The accumulated surfaces in this fixed unit were assumed as the effective surface. This effective surface represented the instantaneous average combustion geometry where the S_{ox}/S_o values were calculated according to it. A modification was added to the second solid phase FORTRAN program to calculate the effective accumulated surface for each propellant formulation then to estimate the S_{ox}/S_o average ratio (Table 5).

To make a reasonable connection between the BDP model and the previous suggestion, Equation (15) was used to calculate the value of h/D_o for each formulation at 20-120 bar followed by correction of the calculated S_{ox}/S_o values that based on $h/D_o \approx 0.25$. The values of t_{ign} were based on C_{ign} value of 190 s $atm^{(0.72)}/cm^{(1.8)}$, as derived by Shannon [18]. Thus, the BDP model principle was partially applied and effect of the measured specific surface areas was prevailed (introduced and corrected). In case of additives incorporation to the AP/PU-binder matrix, α was represented the ratio of the oxidizer to oxidizer-fuel binder combination and the S_{ox}/S_o ratio was modified to the oxidizer to oxidizer-fuel binder combination surface ratio (Table 5). Then, Equation (13) was modified to the following form:

$$m_T = \left(\overline{m_{ox}} / \alpha\right) \times \left(\frac{\overline{S_{ox}}}{\overline{S_{ox}} + S_f} \right) \tag{16}$$

5.3.2 CB incorporation

As a stable material up to about 4000 K, during combustion of the propellant contained CB, it was assumed that CB solid particles were heated up to the propellant surface temperature then leaved the combustion surface with the reacted AP/binder matter to the gas phase with an extremely low burning rate. Thus, Equation (9) was modified to the form:

$$(T_s - T_\circ) \cdot \left(1 + \frac{m_{CB}}{m_T} \cdot \frac{C_{CB}}{C_p}\right) = -\alpha \frac{\overline{Q_L}}{C_p} - (1-\alpha)\frac{Q_{fuel}}{C_p} + 1.25(1-\beta_F)\alpha \times \frac{\overline{Q_{AP}}}{C_p} \exp\left(-\overline{\xi^*_{AP}}\right) \tag{17}$$

The ratio m_{CB}/m_T was replaced by the CB effective loading fraction to the oxidizer-fuel binder combination α_{CB}. Then, Equation (17) was modified to the form:

$$(T_s - T_\circ) \cdot \left(1 + \alpha_{CB} \cdot \frac{C_{CB}}{C_p}\right) = -\alpha \frac{\overline{Q_L}}{C_p} - (1-\alpha)\frac{Q_{fuel}}{C_p} + 1.25(1-\beta_F)\alpha \times \frac{\overline{Q_{AP}}}{C_p} \exp\left(-\overline{\xi^*_{AP}}\right) \tag{18}$$

5.3.3 Al-powder incorporation

Metal combustion does not usually contribute much to the burning rate of the propellant itself because most of the heat release occurs far from the propellant surface. However, as with most generalizations about metal behavior, this one was violated by propellant compositions with oxidizers containing fluorine [27]. The effect of aluminum addition on the burning rate of

propellant is difficult to validate because of the several competing factors that are called into play and any combustion modeling effort in respect of an aluminized propellant has, on necessity, to be based on a specific hypothesis regarding the role of aluminum. While, many of the experimentally proved hypotheses are needy for real burning atmospheres, not oxidizing gases [28]. In addition, a study is cleared that Al not affect AP decomposition [29].
We were assumed that, during aluminized propellant combustion, the aluminum particles were heated up to the propellant surface temperature and melted at the condensed phase. The molten metal was presented in the gaseous phase in an agglomerated state. Its combustion was rather slow, taking place probably at some distance downstream of the gaseous reaction zone of the propellant. This assumption can be applied for the micrometer-size aluminum only because it has been proved that the nanometer-size powder combustion begins at temperatures lower than Al melting point by about 200 to 300 °C [30]. Thus, the assumption suggested by Summerfield for the non-aluminized propellants was also applied for this proposed hypothesis of aluminum combustion. The addition of aluminum powder in any propellant is likely to result in a higher heat flux from the gaseous phase to the solid surface. The increased heat flux increases owing to the steeper temperature gradient, the increased thermal conductivity of the combustion products and the lowered average heat capacity of the solid [28]. When all of these effects were incorporated into Equation (18), it was modified to the following form:

$$(T_s - T_\circ)\cdot\left(1+\frac{m_{Al}}{m_T}\cdot\frac{C_{Al}}{C_p}+\alpha_{CB}\cdot\frac{C_{CB}}{C_p}\right) = -\frac{m_{Al}}{m_T}\cdot\frac{h_f}{C_p}-\alpha\frac{\overline{Q_L}}{C_p}-(1-\alpha)\frac{Q_{fuel}}{C_p}$$
$$+1.25(1-\beta_F)\alpha\times\frac{\overline{Q_{AP}}}{C_p}\exp\left(-\overline{\xi^*_{AP}}\right) \qquad (19)$$

The ratio m_{Al}/m_T was replaced by the Al effective loading fraction to the oxidizer-fuel binder combination α_{Al}. Then, Equation (19) was modified to the form:

$$(T_s - T_\circ)\cdot\left(1+\alpha_{Al}\cdot\frac{C_{Al}}{C_p}+\alpha_{CB}\cdot\frac{C_{CB}}{C_p}\right) = -\alpha_{Al}\cdot\frac{h_f}{C_p}-\alpha\frac{\overline{Q_L}}{C_p}-(1-\alpha)\frac{Q_{fuel}}{C_p}$$
$$+1.25(1-\beta_F)\alpha\times\frac{\overline{Q_{AP}}}{C_p}\exp\left(-\overline{\xi^*_{AP}}\right) \qquad (20)$$

5.3.4 $CaCO_3$ and CC incorporation

Representative methods to control the burning rate of composite propellants used the date including adding a combustion accelerator or moderator. It is well known that the burning rate of these propellants, which contain AP, is enhanced when some transition metal oxides (TMO'S) like CC and Fe_2O_3 used, and reduced with some alkaline salts like LiF, or $CaCO_3$. Although many researchers have proposed various theories as to how the TMO'S enhance the burning rate, the mechanism remains unclear [31]. The same phenomenon accompanies the moderators too [32, 33].
The previous measurement results of the ignition temperatures (Table 3) were assumed as an applicable guide to explore this problem (Figure 4 describes mass loss profiles for some mixtures). The T_{ig} data related to the sudden degradation steps for each mixture showed that, CC addition over the same AP size was effective (lowered the T_{ig}) and became more vigorous with lower AP size. On the other hand, $CaCO_3$ addition over the same AP size was neglected (elevated the T_{ig}) and had a slight effect with lower AP size.
These data reinforced the assumptions that with burning rate accelerators the AP mass flux will be enhanced by lowering the activation energy required to start its regression then increases its sensitivity to heat according to its particle size and accelerator content [31]. In addition, in case of $CaCO_3$, the strong endothermic process (Q_{CaCO3}) to be pertinent to the possible cooling at or just above the combustion surface that results in burning depression [33]. Thus, we were assumed that:

a) $CaCO_3$ particles were heated to the surface temperature then decomposed or leaved and decomposed to CaO very close to the combustion surface. Therefore, solid CaO particles were continued to the gas phase far from the combustion surface. Under this assumption, Equation (20) was modified to the following form:

$$(T_s - T_\circ)\cdot(1+\alpha_{CaCO_3}\cdot\frac{C_{CaCO_3}}{C_p}+\alpha_{Al}\cdot\frac{C_{Al}}{C_p}+\alpha_{CB}\cdot\frac{C_{CB}}{C_p}) = -F_{CaCO_3}\cdot\frac{Q_{CaCO_3}}{C_p}-\alpha_{Al}\cdot\frac{h_f}{C_p}-\alpha\frac{\overline{Q_L}}{C_p}$$
$$-(1-\alpha)\frac{Q_{fuel}}{C_p}+1.25(1-\beta_F)\alpha\times\frac{\overline{Q_{AP}}}{C_p}\exp\left(-\overline{\xi^*_{AP}}\right) \quad (21)$$

Where:

$$F_{CaCO_3} = \frac{M_{CaO}}{M_{CaCO_3}}\cdot\alpha_{CaCO_3} \quad (22)$$

b) CC ultra fine particles (0.75 µm) were covered the AP particles and both of them heated to the surface temperature. Under its catalytic effects, CC leaded to AP decomposition with higher mass flux. Therefore, CC particles were ejected to the gas phase far from the surface. Then, Equations (21 and 2) were modified to the following forms:

$$(T_s - T_\circ)\cdot(1+\alpha_{CC}\cdot\frac{C_{CC}}{C_p}+\alpha_{CaCO_3}\cdot\frac{C_{CaCO_3}}{C_p}+\alpha_{Al}\cdot\frac{C_{Al}}{C_p}+\alpha_{CB}\cdot\frac{C_{CB}}{C_p}) = -F_{CaCO_3}\cdot\frac{Q_{CaCO_3}}{C_p}$$
$$-\alpha_{Al}\cdot\frac{h_f}{C_p}-\alpha\frac{\overline{Q_L}}{C_p}-(1-\alpha)\frac{Q_{fuel}}{C_p}+1.25(1-\beta_F)\alpha\times\frac{\overline{Q_{AP}}}{C_p}\exp\left(-\overline{\xi^*_{AP}}\right) \quad (23)$$

$$\overline{m_{ox}} = \sum_{i=1}^{n}\alpha_{ox_i}A_{ox_i}\exp\left(-E_{ox_i}\cdot F_{CC_i}/RT_s\right) \quad (24)$$

The factor F_{CCi} was evaluated on the basis of the previous T_{ig} data and defined as the ratio of T_{ig} measured for (7.5% CC × 62.5% AP) to T_{ig} measured without CC. To make a connection to our requirements, the relationship between AP particle sizes [X (µm)] and the measured specific surface areas [Y (m^2/g)] by the BET-method was fitted to:

$$Y = 1.732032\ X^{-0.4952952} \rightarrow R^2 = 0.9994 \quad (25)$$

In addition, the relationship between AP specific surface areas [X (m^2/g)] and F_{CCi} [Y] was fitted to:

$$Y = 0.9366\ exp(-0.2437\ X) \rightarrow R^2 = 0.9997 \quad (26)$$

Thus, to apply for any formulation with known AP_i specific surface area, the new F_{CCi} value (say F^*_{CCi}) corresponded to any other effective CC fraction (CC_{ef}), → (CC% × AP_i%), value (say CC^*_{ef}) was obtained by:

$$F^*_{CC_i} = F_{CC_i} - [(CC_{ef} - CC^*_{ef})\cdot(F_{CC_i} - 1.0)/CC_{ef}] \quad (27)$$

5.4 Ballistic properties evaluation

According to what mentioned, the independent ballistic properties that would be separately inspected were the linear burning rate (after T_s estimation) and the temperature sensitivities. In addition, the dependent ballistic property that might be corrected was the pressure index (n). The value of n was evaluated, at least, from the predicted burning rates at three pressure values (20, 70 and 120 bar). It was assumed that the formulations obeyed the De Saint Robert and Vieille law. The propellant temperature sensitivity of burning rate at assigned pressure σ_{Pc} was calculated under, (70 bar as the particular value of pressure), the assumption that its value not changed at upper or lower temperature conditions when compared to the reference temperature T_o. Then, the propellant temperature sensitivity of pressure at assigned blocking π_{KL} was calculated, $\pi_{KL} = \sigma_{Pc} / 1- n$. The applied techniques to deal with the ballistic properties were:

1) To deal with r, the previously mentioned schemes were used, and iterative techniques were applied to estimate the propellant surface temperature in two steps. The first represented the preliminary approach and was applied between T_o and T_f where the convergence yielded

the first value of the surface temperature T_s (say T_{1s}). The second represented the final approach, where T_d was estimated (between T_o and T_{1s}) then T_{fs} was calculated followed by solid and gas phases specifications corrections, and was re-applied between T_o and T_f where the convergence yielded the second value of the surface temperature T_s (say T_{2s}). Thus, the surface temperature T_s was assumed to approximately equal the average value between T_{1s} and T_{2s}.

2) To deal with σ_{Pc}, the following approach was applied [20, 34]:

a) Because the regression of the oxidizer was considered as the rate-controlling step in combustion then σ_{Pc} basic definition was simplified, under an initial temperature T_o and pressure $P_c \approx 70$ bar, to:

$$\sigma_{P_c} = \frac{d \ln \overline{m_{ox}}}{dT_o} \tag{28}$$

b) By differentiating Equations (2, 3, and 10) and solving for σ_{Pc} in Equation (28), we obtained:

$$\sigma_{P_c} = \frac{1 + (1.25)(1-\beta_F)\left(\frac{\overline{Q_{AP}}}{C_p}\right)\cdot\alpha\cdot\overline{\xi^*_{AP}}\cdot\exp\left(-\overline{\xi^*_{AP}}\right)\left(\frac{\overline{E_{ox}}}{RT^2_{AP}}\right)}{\frac{RT_s^{\,2}}{\overline{E_{ox}}} + (1.25)(1-\beta_F)\left(\frac{\overline{Q_{AP}}}{C_p}\right)\cdot\alpha\cdot 2\overline{\xi^*_{AP}}\cdot\exp\left(-\overline{\xi^*_{AP}}\right)} \tag{29}$$

Where:

$$\overline{E_{ox}} = \sum_{i=1}^{n} \alpha_{ox_i} E_{ox_i} \tag{30}$$

3) If the calculated $n \geq 0.77$ then, it was corrected in an analogous manner to σ_{Pc} [20]:

$$n = \frac{d \ln \overline{m_{ox}}}{d \ln P} = \delta \Big/ \left\{ 2 + \left[\left(\frac{RT_s^{\,2}}{\overline{E_{ox}}} \right) \Big/ (1.25)(1-\beta_F)\left(\frac{\overline{Q_{AP}}}{C_p}\right)\cdot\alpha\cdot\overline{\xi^*_{AP}}\cdot\exp\left(-\overline{\xi^*_{AP}}\right) \right] \right\} \tag{31}$$

A FORTRAN computer program was established for obtaining, by the previously described schemes, the linear burning rates and surface temperatures of the twenty Butalites formulations under this investigation. The propellant ingredients with their basic specifications represented the program main input data. The combustion equations were solved iteratively and no particular difficulty was encountered in the solution convergence. The program was compiled and applied to calculate the propellant surface temperature, linear burning rate and other ballistic properties.

6 Discussions

The specific surface areas of the solid ingredients (Table 2) were effective, especially, when compared with their theoretically calculated values. The ignition temperatures (Table 3) clarified that CC had the greatest effect and other ingredients effects (± 2%) can be neglected. The thermal analytical measurements (Table 2) showed that the AP samples, (PU-binder samples), kinetic parameters at high and low conversions were in acceptable agreements with some important literature [7, 22 and 35]. Plasticizer addition to the binder formulation had the greatest effect on lowering the decomposition characteristic parameters. The higher the AP particle size the lower the decomposition kinetic parameters and the higher the automatically determined heats of gasification. The kinetic parameters variations at high conversion for both AP [11] and PU-binder were introduced to the modified BDP model equations in this study. The ballistic properties (Tables 1 and 7) were discussed according to factors affecting combustion as follows:

1) The investigations for sub-group AI and sub-group BI showed the trend of increasing the linear burning rate when increasing AP content. Similar behavior was observed in all

pressures from 20 to 120 bar. That was demonstrated due to the increase of the oxidizer volumetric solid loading through the propellant microstructure, the increase of the reaction ability to be more exothermic, and the increase of the propellant surface temperature.

2) The investigations for sub-group AII and sub-group BII showed a monotonous decrease in the burning rate when increasing the particle size in all inspected pressures due to the decrease of the oxidizer burning surface area.
3) For Sub-group AIII, Al was found to have a remarkable effect on the linear burning rate. The effect was similar in all pressures revealing an effective increase with Al content when compared to the burning rates evaluated for the non-aluminized fuel rich formulation AI-3. This latter phenomenon is not known for regular propellants where burning rates are not much affected by Al presence (added at the expense of the oxidizer) and may be attributed to Al appreciable influence on the flame temperature [36, 37].
4) For Sub-group AIV and Sub-group AV, effect of the burning rate accelerator (CC) was investigated. CC exhibited a moderate increase in the evaluated linear burning rate for the non-Al-formulations (AIV) due to the exothermic reaction at the CC-AP interface which lowered the oxidizer ignition temperature, increased its sensitivity to heat, reduced the activation energy required to start the deflagration reaction on the propellant surface and consequently increased the reaction rate through the propellant solid-gas interface. However, CC exhibited sharp increase in the burning rates when changing to Al-formulations (AV), due to Al additional effect.
5) For Sub-group BIII, effect of CC and $CaCO_3$ addition was compared. BIII-3 formulation predictions were marked as coincident with its practical results at 25 ºC, which reinforced $CaCO_3$ treatment methodology.
6) Formulation BIV revealed that the prediction ability of the ballistic properties for an independent high burning rate propellant formulation was verified.

Table 7 Formulations predicted data and their prediction accuracy levels

No.	T_s (K)			Parameter	n	Mean σ_{P_c} (/ºC)	r (mm/s)				
							-30 ºC	25 ºC			50 ºC
	20 bar	*70 bar*	*120 bar*				70/bar	20/bar	70/bar	120/bar	70/bar
				Practical:	0.120	0.01300			0.260	0.277	0.360
AI-1	*298.1*	*590.0*	*645.5*	Theoretical:	0.226	0.00943	0.165	0.208	0.277	0.313	0.350
				Accuracy (%):	**+88.3**	**-27.5**			**+6.5**	**+13.0**	**-2.8**
				Practical:	0.270	0.00360		0.378	0.530	0.613	0.580
AI-2	*380.8*	*805.5*	*833.4*	Theoretical:	0.267	0.00439	0.387	0.353	0.493	0.569	0.550
				Accuracy (%):	**-1.1**	**+21.9**		**-6.6**	**-7.0**	**-7.2**	**-5.2**
				Practical:	0.340	0.00565	0.790	0.725	1.110	1.333	1.260
AI-3	*430.9*	*813.3*	*836.2*	Theoretical:	0.335	0.00401	0.815	0.668	1.016	1.217	1.123
				Accuracy (%):	**-1.5**	**-29.0**	**+3.2**	**-7.9**	**-8.5**	**-8.7**	**-10.9**
				Practical:	0.280	0.00660		0.711	1.010	1.175	1.190
AII-1	*437.9*	*817.3*	*839.1*	Theoretical:	0.347	0.00388	0.777	0.623	0.962	1.159	1.060
				Accuracy (%):	**+23.9**	**-41.2**		**-12.4**	**-4.8**	**-1.4**	**-10.9**
				Practical:	0.310	0.00550		0.604	0.890	1.052	1.020
AII-2	*445.0*	*821.0*	*842.0*	Theoretical:	0.360	0.00377	0.694	0.544	0.854	1.036	0.938
				Accuracy (%):	**+16.1**	**-31.5**		**-9.9**	**-4.0**	**-1.5**	**-8.0**
				Practical:	0.260	0.00690	2.170	1.848	2.560	2.945	2.820
AIII-1	*640.9*	*868.2*	*880.6*	Theoretical:	0.257	0.00289	2.329	1.979	2.730	3.135	2.935
				Accuracy (%):	**-1.2**	**-58.1**	**+7.3**	**+7.1**	**+6.6**	**+6.5**	**+4.1**
				Practical:	0.220	0.00180	3.820	3.150	4.150	4.672	4.370
AIII-2	*807.0*	*895.1*	*905.1*	Theoretical:	0.203	0.00260	3.525	3.151	4.066	4.537	4.338
				Accuracy (%):	**-7.7**	**+44.4**	**-7.7**	**+0.03**	**-2.0**	**-2.9**	**-0.7**
				Practical:	0.230	0.00560	1.420	1.282	1.710	1.936	2.080
AIV-1	*502.9*	*822.6*	*837.5*	Theoretical:	0.170	0.00332	1.506	1.461	1.807	1.980	1.963
				Accuracy (%):	**-26.1**	**-40.7**	**+6.1**	**+14.0**	**+5.7**	**+2.3**	**-5.6**
				Practical:	0.280	0.00570	1.850	1.662	2.360	2.744	2.810
AIV-2	*580.5*	*816.1*	*827.7*	Theoretical:	0.283	0.00307	2.120	1.761	2.510	2.923	2.710
				Accuracy (%):	**+1.1**	**-46.1**	**+14.6**	**+6.0**	**+6.4**	**+6.5**	**-3.6**
				Practical:	0.190	0.00285	2.670	2.483	3.150	3.490	3.370
AV-1	*719.3*	*853.8*	*864.5*	Theoretical:	0.307	0.00281	2.874	2.284	3.354	3.957	3.598
				Accuracy (%):	**+61.6**	**-1.4**	**+7.6**	**-8.0**	**+6.5**	**+13.4**	**+6.8**
				Practical:	0.200	0.00280	3.290	2.919	3.750	4.177	4.060
AV-2	*747.3*	*833.2*	*842.7*	Theoretical:	0.309	0.00277	3.500	2.768	4.076	4.814	4.368
				Accuracy (%):	**+54.5**	**-1.1**	**+6.4**	**-5.2**	**+8.7**	**+15.3**	**+7.6**
				Practical:	0.340			4.448	6.810	8.180	
BI-1	*876.5*	*945.3*	*954.4*	Theoretical:	0.300	0.00221	6.363	4.933	7.187	8.450	7.596
				Accuracy (%):	**-11.8**			**+10.9**	**+5.5**	**+3.3**	
				Practical:	0.390			4.540	7.400	9.131	
BI-2	*883.7*	*952.6*	*961.8*	Theoretical:	0.416	0.00218	7.187	4.814	8.103	10.138	8.557
				Accuracy (%):	**+6.7**			**+6.0**	**+9.5**	**+11.0**	
				Practical:	0.440			5.786	10.040	12.727	
BI-3	*891.7*	*961.0*	*970.3*	Theoretical:	0.464	0.00215	8.247	5.191	9.280	11.914	9.791
				Accuracy (%):	**+5.5**			**-10.3**	**-7.6**	**-6.4**	
				Practical:	0.310	0.00132	6.270	4.578	6.750	7.978	6.980
BII-1	*892.9*	*963.6*	*972.9*	Theoretical:	0.352	0.00211	6.319	4.568	7.097	8.578	7.482
				Accuracy (%):	**+13.5**	**+59.8**	**+0.8**	**-0.2**	**+5.1**	**+7.5**	**+7.2**
				Practical:	0.280	0.00127	6.890	5.197	7.380	8.582	7.620
BII-2	*891.7*	*962.1*	*971.4*	Theoretical:	0.363	0.00212	6.502	4.635	7.307	8.888	7.705
				Accuracy (%):	**+29.6**	**+66.9**	**-5.6**	**-10.8**	**-1.0**	**+3.6**	**+1.1**
				Practical:	0.400	0.00208	6.920	4.695	7.750	9.615	8.160
BIII-1	*882.6*	*950.7*	*959.7*	Theoretical:	0.301	0.00219	6.703	5.186	7.560	8.890	7.985
				Accuracy (%):	**-24.8**	**+5.3**	**-3.1**	**+10.5**	**-2.5**	**-7.5**	**-2.1**
				Practical:	0.370	0.00159	10.960	7.517	11.950	14.587	12.430
BIII-2	*877.8*	*945.5*	*954.5*	Theoretical:	0.277	0.00213	10.669	8.478	11.996	13.928	12.652
				Accuracy (%):	**-25.1**	**+34.0**	**-2.7**	**+12.8**	**+0.4**	**-4.5**	**+1.8**
				Practical:	0.300	0.00082	6.860	4.931	7.180	8.440	7.330
BIII-3	*878.7*	*946.7*	*955.8*	Theoretical:	0.306	0.00220	6.331	4.868	7.144	8.427	7.548
				Accuracy (%):	**+2.0**	**+168.3**	**-7.7**	**-1.3**	**-0.5**	**-0.2**	**+3.0**
				Practical:	0.230			13.449	17.940	20.308	
BIV	*866.6*	*934.0*	*943.0*	Theoretical:	0.341	0.00205	16.627	12.143	18.613	22.368	19.593
				Accuracy (%):	**+48.3**			**-9.7**	**+3.8**	**+10.1**	

The previous table provided us with complete visions about the accuracy levels accompanied our predictions. Generally, the all-ballistic properties predictions were marked as approved. Some of n and σ_{Pc} predicted results, as a variation behavior, were marked as fair. Many of

them (64%) as specific values for comparison with the experimental results may be marked as not fair, but when inspected their effects over the predicted linear burning rates at different temperatures (-30, 25 and 50 ºC) and pressures (20-120 bar) they were marked as applicable. Therefore, following the international acceptance margins [8, 22] that based on the direct comparisons between the theoretically predicted and practically evaluated linear burning rates at 70 bar represented the best way to judge validity of the ballistic properties predictions. Evidently, the prediction accuracy levels were listed in Table 7.

From the modifications applied to the BDP model, it was very important to clarify the following:

1) The modified model really liberated itself from its emphasis on the flame standoff distances under the assumption suggested by Summerfield et al [20, 24]. However, under this assumption (to guaranteed iterations continuation over the model equations until convergences) Q_L values were introduced in negative form [17, 18, 21 and 22], and C_P and λ assumed to equal the half-average values calculated before for solids and gases combination.
2) The predicted densities (Table 5) were within deviations from about -2.7 to +0.9% when compared to the practical results (Table 1) which provided them with the required certainty.
3) The determined pre-exponential factor in "s^{-1}" for AP, (PU-binder), samples was assumed to have the same values when converted to mass flux in "g cm^{-2} s^{-1}" because the evaluated kinetic parameters under high conversion conditions were close together.
4) The pressure value of 70 bar represented the standard condition value in this study where many specific parameters were characterized (like, K_{AP} [3, 17 and 18], C_{ign} [18]… etc.). In addition, under this pressure value with variant equivalence ratios, the instantaneous regression rates of pyrolysis for both AP-oxidizer and hydrocarbon-fuel binders are intrinsically oscillated about a single value or approximately coincident together. Where, the overall ratio of their regression rates tends to unity suggesting that the pyrolysis of the mixture approaches a steady state situation [38]. Moreover, it represents the international value at which the propellant specifications are characterized and compared (70 bar ≈ 70 atm ≈ 1000 psi) [8, 36].
5) The used one-dimensional limited temperature profile with variant decomposition characteristic parameters to estimate T_s verified the requirements leaded to predict the ballistic properties. Herein, we considered that, some T_s values in Group-A compositions, especially at 20 bar (Table 7), were said to be an art rather than a science.

7 Conclusions

Solid and gas phases calculations provided the study objective with the required light for its solution convergence. The linear burning rate predictions, without the BDP model multiple flame standoff distances, were verified using an easy abstention technique over the combustion zone. The used reference data of β_F verified applicable reflections to the overall pattern but still require separate investigations over AP/HTPB-based PU-binder formulations. The S_{ox}/S_o ratios calculation and correction base, verified passable (moderate extent) reflections to the predicted linear burning rates. They require wider calculations for the all h/D_o ratios regime and deeper penetration to the propellant surface geometry at different pressures under microscopic levels. The additives (Al, CB, CC, and $CaCO_3$) passive incorporation methodology to the BDP model was marked as fair. The predicted linear burning rates were verified the international acceptance margins in this field [8, 22]. Evidently, about 98% of the results were within ± 15% deviation, 81% within ± 10%, and 43% within ± 6% at 25 ºC and 20-120 bar. In addition, 100% were within ± 10% deviation and 56% within

± 6% at 25 ºC and 70 bar. Moreover, 100% were within ± 15% deviation, 89% within ± 10%, and 54% within ± 6% at -30 ºC, +50 ºC and 70 bar. The international acceptance margins [8] between linear burning rate theoretical predictions and practical evaluations at 70 bar were verified for the whole Butalites formulations under this investigation, about 94% of the all-70 bar predictions were within ± 10% error range. The pressure index and temperature sensitivities prediction values were applicable for the preliminary studies. The verified accuracy levels provided us with the required information about the used technique validity and the applied modifications applicability to the basic BDP model [17], especially, if compared to similar studies [20-22].

References

[1] G. P. Sutton, Rocket Propulsion Elements, Sixth Edition, New York: John Wiley & Sons, Inc. (1992) Chapter 13.

[2] Y. Timnat, Advanced Chemical Rocket Propulsion, London: Academic Press (1987) Chapter 3.

[3] K. Kuo, M. Summerfield, Fundamentals of Solid Propellant Combustion, New York: AIAA, Inc. (1984) Chapter 8.

[4] H. Singh, H. Shekhar, Problems Associated with the Combustion Modeling of Solid Rocket Propellants, Printed by Printwell, India (2008).

[5] Solid propellant selection and characterization, NASA SP-8064, Space Vehicle Design Criteria, NASA, Washington, DC, USA (1971).

[6] A. Davenas, Solid Rocket Propulsion Technology, Oxford: Pergamon Press (1993) Chapter 4.

[7] G. Lengellé, J. Duterque, J.F. Trubert, Combustion of Solid Propellants, RTO-EN-023, ONERA, France (2004).

[8] T. Deyu, Z. Wei, Burning Rate Estimation of AP/AL/HTPB Propellants, Germany, ICT (1989) 54-1: 54-4.

[9] A. Davenas, Solid Rocket Propulsion Technology, Oxford: Pergamon Press (1993) Chapter 10.

[10] P. Simon, Isoconversional methods: Fundamentals, Meaning and Application, Thermal Analysis and Calorimetry (2004) 76: 123-132.

[11] Abdel-Wareth W. M., X. Xu, Ammonium Perchlorate Decomposition Characteristic Parameters Determination, A Simplified Approach, India, New Delhi, International Conference on Mechanical and Aerospace Engineering, March 21-23 (2011) 570-574.

[12] S. I. Stoliarov, R. N. Walters, Determination of the Heats of Gasification of Polymers Using DSC, DOT/FAA/AR-TN07/62, SRA International, Inc., USA (2007).

[13] C. L. Yaws, Handbook of Thermal Conductivity, Inorganic Compounds and Elements, Volume 4, Gulf Publishing Company (1995).

[14] M. Binnewies, E. Milke, Thermo-chemical Data of Elements and Compounds, Germany: Wiley-Vch Publishing Co. (2002).

[15] P. Heira, J. Campos, Some Rules for the Design of High Solid Loading Composite Solid Propellants, Germany, ICT (1995) 55-1: 55-14.

[16] S.Gordon, B.J. Mcbride, Computer Program for Calculation of Complex Chemical Equilibrium Compositions and Applications, NASA RP 1311, Part II: Users Manual and Program Descriptions, USA (1996).

[17] M. W. Beckstead, R. L. Derr, C. F. Price, A Model of Composite Solid-Propellant Combustion Based on Multiple Flames, AIAA Journal (1970) 8 (12): 2200-2207.

[18] M. Iqbal, W. Liang, Propellant Burning Rate Calculations with Improved Predictions, Chinese Journal of Solid Rocket Technology (2002) 25 (1): 51-54.

[19] M. Nikazar, M. B. Bagherpour, B. Dabir, The Use of Fractal for Prediction of Burning Rate of Composite Solid Propellants, Journal of Thermal Science (2000) 9 (4): 361-364.

[20] V. Swaminathan, M. Soosaimarian, Burning Rate Evaluation of Composite Solid Propellants - A Simplified Approach, Propellants and Explosives (1981) 6: 37-41.

[21] M. Iqbal, W. Liang, Burning Rate Calculations of Wide Distribution Ammonium Perchlorate Composite Propellants, AIAA (2006-1161).

[22] L. Shi-liang, Study on Primary Combustion Characteristics of Magnesium-based Hydro-reactive Metal Fuel Used for Water Ramjet, National University of Defense Technology, Changsha, Hunan, P.R.China, Ph. D. Thesis, Nov. (2009).

[23] N. Kubota, Thermo-Chemical Aspects of Combustion, Germany: Wiley-Vch Publishing Co. (2002) Chapter 3.

[24] J. A. Steinz, P. L. Stang, M. Summerfield, The Burning Mechanism of Ammonium Perchlorate-Based Composite Solid Propellants, Aerospace and Mechanical Science Report No. 830, Princeton University (1969).

[25] D. Baker, Investigation of Composite Solid Propellant Burning Rate Temperature Sensitivity, Ph. D. Thesis, Purdue University (1973).

[26] S. Krishnan, R. Jeenu, Combustion Characteristics of AP/HTPB Propellants with Burning Rate Modifiers, Journal of Propulsion and Power (1992) 8 (4): 748-755.

[27] K. Kuo, M. Summerfield, Fundamentals of Solid Propellant Combustion, New York: AIAA, Inc. (1984) Chapter 9.

[28] T. Bazyn, H. Krier, N. Glumac, Oxidizer and Pressure Effects on the Combustion of 10-µm Aluminum Particles, Journal of Propulsion and Power (2005) 21 (4): 577-581.

[29] J. Zhi, W. Tian-Fang, L. Shu-Fen, Z. Feng-Qi, L. Zi-Ru, Y. Cui-Mei, L. Yang, L. Shang-Wen, Z. Gang-Zhui, Thermal Behavior of Ammonium Perchlorate and Metal Powders of Different Grades, Thermal Analysis and Calorimetry (2006) 85 (2): 315-320.

[30] J. Bouillard, A. Crossley, J. Dien, P. Dobson, T. Klepping, A. Vignes, Safety Parameter Characterization Techniques for Nanoparticles, DR-152-200802-2, European Union (2008).

[31] K. Fujimura, A. Miyaka, The Effect of Specific Surface Area of TiO2 on the Thermal Decomposition of Ammonium Perchlorate, Thermal Analysis and Calorimetry (2010) 99: 27-31.

[32] L. Zivorad, Burning Rate of a Tri-modal Composite Rocket Propellant, J. Propulsion (1990) 6 (5): 515-518.

[33] X. Xingcai, W. Zhujun, Research on Lowering the Pressure Exponent of HTPB Propellant at High Pressure, Journal of Propulsion Technology (1993) (6): 73-76.

[34] N. Cohen, D. Flanigan, Mechanisms and Models of Solid Propellant Burn Rate Temperature Sensitivity - A Review, AIAA (1984-0286).

[35] K. N. Ninan, K. Krishnan, Thermal Decomposition Kinetics of Polybutadiene Binders, J. Spacecraft (1982) 19 (1): 92-94.

[36] Abdel-Wareth W. M, Study of the Combustion Behavior of the Low Oxygen Content CSRP, Cairo University, Faculty of Engineering, Cairo, Egypt, M. Sc. Thesis (2006).

[37] A. Shalom, A. Gany, Flammability Limits and Ballistic Properties of Fuel-Rich Propellants, Propellants, Explosives, Pyrotechnics (1991) 16: 59-64.

[38] Preetham, S. R. Chakravarthy, Effect of Heterogeneity of Solid Propellants on Their Intrinsic Stability of Pyrolysis, AIAA (2004-240).

Appendix 1

1) AP particle size [x (μm)] and heat of gasification [y (cal/g)]:
$$y = 4.0641\text{Ln}(x) + 95.071 \rightarrow R^2 = 0.89$$
2) PU-binder NCO/OH ratio [x] and heat of pyrolysis [y (cal/g)]:
$$y = -17.3x + 292 \rightarrow R^2 = 1$$
3) PU-binder IM/OH ratio [x] and heat of pyrolysis [y (cal/g)]:
$$y = -21.6x + 285.5 \rightarrow R^2 = 1$$
4) PU-binder DOZ/HTPB ratio [x] and heat of pyrolysis [y (cal/g)]:
$$y = -271.2x + 274.7 \rightarrow R^2 = 1$$
5) AP specific surface [x (μm)] and activation energy [y (kcal/mole)]:
$$y = 0.3723\text{Ln}(x) + 27.336 \rightarrow R^2 = 0.9783$$
6) AP specific surface [x (μm)] and pre-exponential factor [y (/s)]:
$$y = 10^6.(1.1588\text{Ln}(x) + 5.7905) \rightarrow R^2 = 0.9831$$
7) PU-binder NCO/OH ratio [x] and activation energy [y (kcal/mole)]:
$$y = -0.33x + 45.59 \rightarrow R^2 = 1$$
8) PU-binder NCO/OH ratio [x] and pre-exponential factor [y (/s)]:
$$y = 10^{11}.(-0.61x + 4.31) \rightarrow R^2 = 1$$
9) PU-binder IM/OH ratio [x] and activation energy [y (kcal/mole)]:
$$y = -0.48x + 45.5 \rightarrow R^2 = 1$$
10) PU-binder IM/OH ratio [x] and pre-exponential factor [y (/s)]:
$$y = 10^{11}.(-0.92x + 4.16) \rightarrow R^2 = 1$$
11) PU-binder DOZ/HTPB ratio [x] and activation energy [y (kcal/mole)]:
$$y = -2.96x + 45.26 \rightarrow R^2 = 1$$
12) PU-binder DOZ/HTPB ratio [x] and pre-exponential factor [y (/s)]:
$$y = 10^{11}.(-5.12x + 3.7) \rightarrow R^2 = 1$$

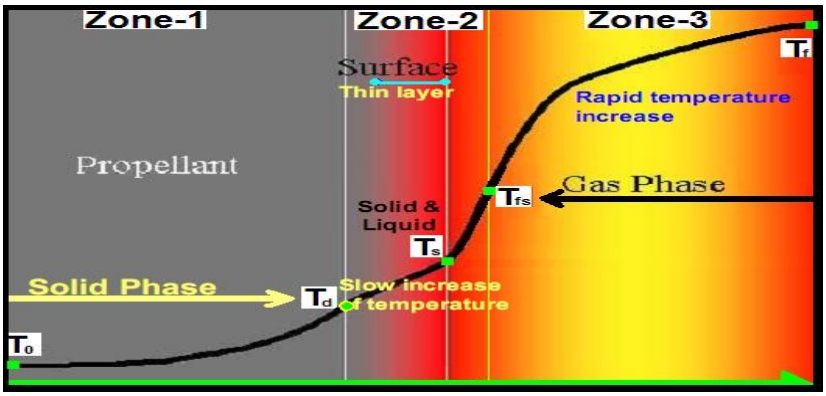

Figure 1 Modified combustion wave of an AP-based composite propellant.

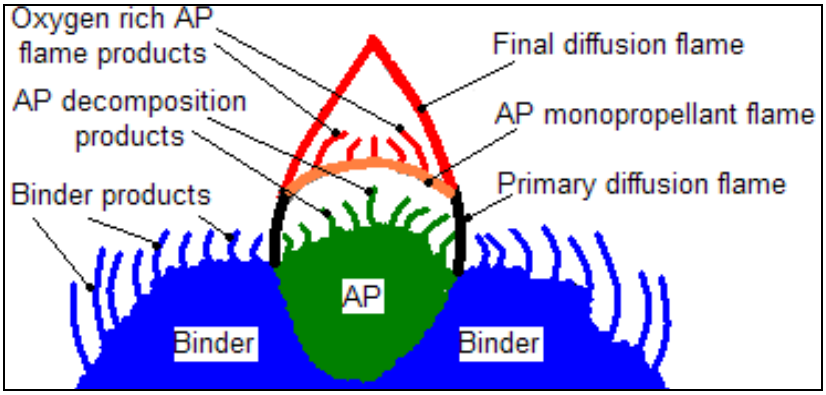

Figure 2 Multiple flames in the BDP model.

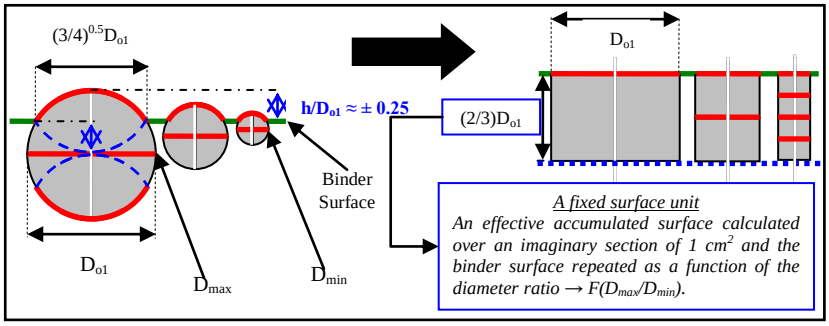

Figure 3 AP-particles, assumed idealized geometry.

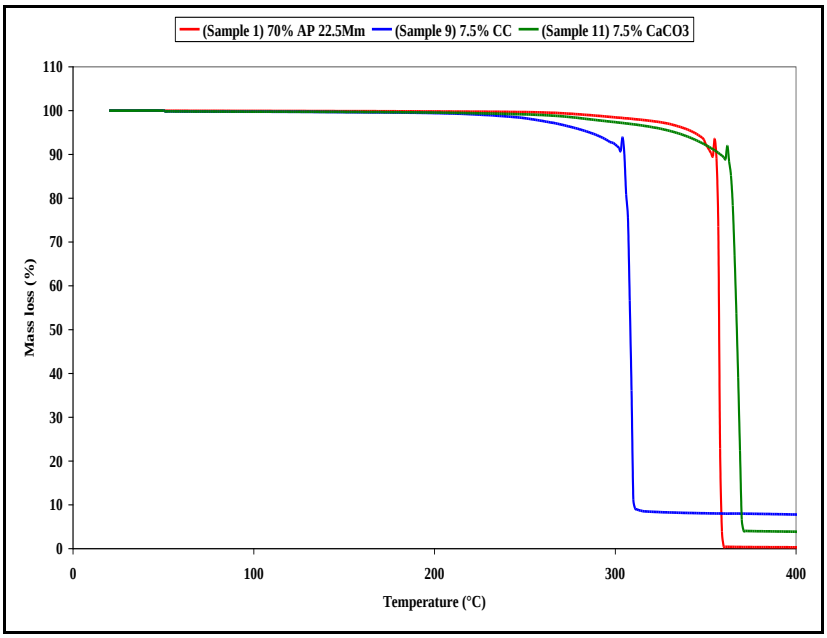

Figure 4 Mass sudden degradation steps (T_{ig}) of some propellant mixtures.

Nomenclature

A_f	Binder Pre-exponential factor
A_{ox}	Oxidizer Pre-exponential factor
C_{Al}	Al specific heat capacity
C_{AP}	AP averaged specific heat
C_{CaCO3}	$CaCO_3$ specific heat capacity
C_{CB}	CB specific heat capacity
C_{CC}	CC specific heat
C_{ign}	Delay constant
C_P	Average heat capacity for the solids and the gases
E_{ox}	Oxidizer activation energy
E_f	Binder activation energy
F_{CCi}	The i^{th}-grade oxidizer mass flux modification factor based on CC incorporation
h_f	Al heat of fusion
M_{CaO}/M_{CaCO3}	CaO to $CaCO_3$ molecular weight ratio (≈ 0.56)
m_{Al}	Al mass flux
m_{CB}	CB mass flux
m_f	Fuel binder mass flux
m_{ox}	Oxidizer mass flux
m_T	Total mass flux of the propellant
n	Propellant pressure index
ox_i	AP grade (i) with pre-defined Sauter mean diameter D_{oi}
$P = P_c$	Combustion pressure
Q_{AP}	Heat release associated with the AP flame conditions
Q_{CaCO3}	$CaCO_3$ heat of decomposition to CaO
Q_{FF}	Heat release associated with the final flame conditions
Q_{fuel}	Heat of pyrolysis of the fuel binder

Q_L	Heat of gasification of the oxidizer
Q_{PF}	Heat release associated with the primary flame
R	Universal gas constant
r	Linear burning rate
r_f	Binder-burning rate
r_{ox}	Oxidizer-burning rate
S_f	Fuel binder surface area
S_o	Total surface area of the propellant
S_{ox}	Oxidizer surface area
T_{AP}	AP adiabatic flame temperature
t_{ign}	AP ignition delay time
ΔH_{fuel}	Fuel binder enthalpy of formation
α	Oxidizer weight fraction
α_{CaCO3}	$CaCO_3$ effective loading fraction to the oxidizer-fuel binder combination
α_{CC}	CC effective loading fraction to the oxidizer-binder combination
α_{oxi}	The i^{th}-grade oxidizer fraction of the total oxidizer in the propellant formulation
β_F	Fraction of the oxidizing reactants that react in the primary diffusion flame
ρ_f	Fuel binder density
ρ_{ox}	Oxidizer density
ρ_P	Propellant density
ξ^*_{AP}	AP flame non-dimensional standoff distance
ξ^*_{FF}	Final flame non-dimensional standoff distance
ξ^*_{PF}	Primary flame non-dimensional standoff distance
λ	Thermal conductivity (average of solids and gases)